20th Australasian Fluid Mechanics Conference
Perth, Australia
5-8 December 2016

Study of Side Force on Slender Hulls in a Cross Flow

S.-K. Lee[1,2]

[1]Defence Science and Technology Group, Melbourne, VIC 3207 AUSTRALIA

[2]University of Tasmania, Launceston, TAS 7250 AUSTRALIA

Abstract

The presence of cross flow on a slender hull can exert a side force which affects the motion control of the hull. For various streamlined vehicles including airships and submersibles, an understanding of the cross flow is key to establishing the aft-body flow field and its effect on propulsion and manoeuvre. In this study, the relation between the side force acting on the hull and the moment of vorticity at the tail plane of the hull is used to develop an analytical-empirical model to interpret the cross flow. The interpretation includes the effect of Reynolds number, fineness ratio, roll rate, experimental hull-support structure (pylon) interference, and deck orientation.

Introduction

From slender-body theory, Jeans [1] showed that the side force acting on a slender hull at incidence (angle $|\psi| > 0$ in the y direction; figure 1) can be expressed as

$$\mathrm{F}_{y,h} = \rho U_\infty \cos(\psi) \int_0^L di_{y,h}(x), \tag{1}$$

where $i_{y,h}(x = L)$ defines the moment of body-axis vorticity (ω_x) about the normal (z) axis at the *tail plane*:

$$i_{y,h}(L) = \int_{-\infty}^{\infty}\int_{-\infty}^{\infty} (\omega_x z)\, dydz. \tag{2}$$

In this study, it is assumed that *all* vorticity is shed from the hull and gets concentrated into identifiable vortices as shown in figure 1, where each vortex has circulation Γ and its centre of rotation is at a normal location z_c, so that Eq. (2) may be recast as

$$i_{y,h}(L) = \Sigma\left(\Gamma \times z_{c,\mathrm{aft}}\right). \tag{3}$$

Now let the circulation of each vortex scale with the cross-flow velocity, $U_\infty \sin(\psi)$, and the maximum radius, r_m, of the hull, i.e.

$$\Gamma = \kappa \times r_m U_\infty \sin(\psi), \tag{4}$$

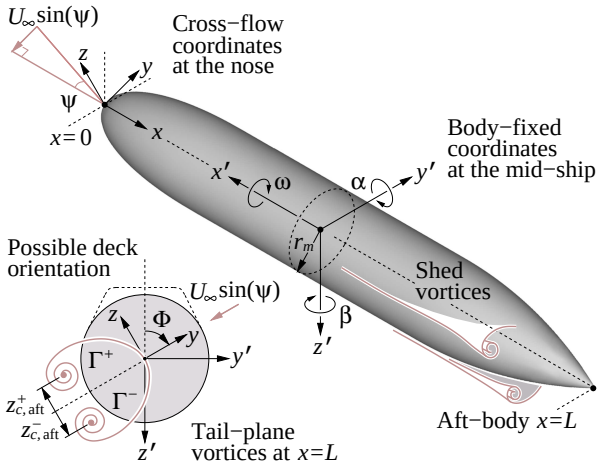

Figure 1. Schematic diagram of a generic slender hull at incidence with parameter definitions and coordinate systems.

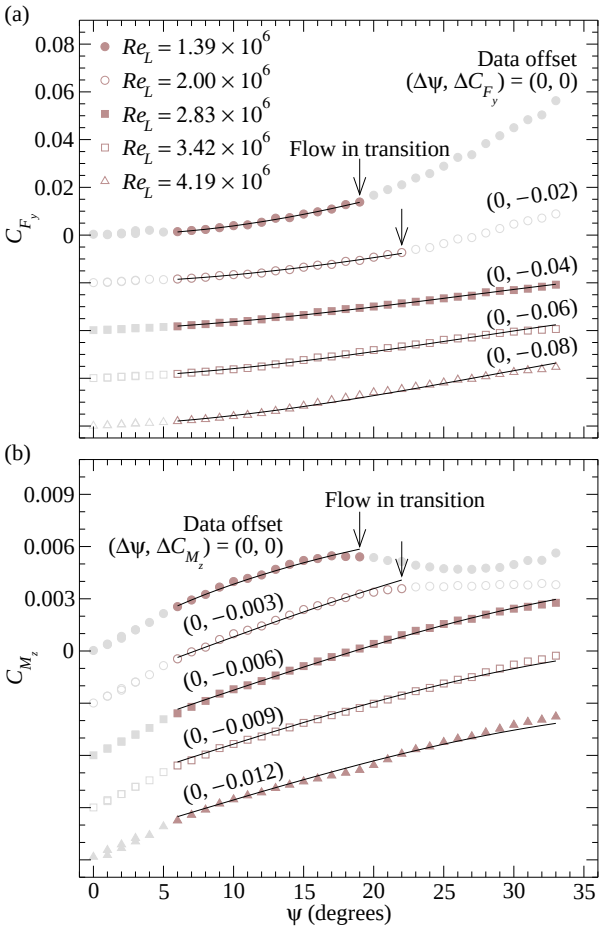

Figure 2. Examples of side-force and yaw-moment coefficients (solid lines) calibrated by using Ahn's [2] wind-tunnel data points for a 6-to-1 prolate spheroid. The calibration of Eqs. (5) and (6) is obtained by curve fitting K and K_h as functions of yaw angle (ψ), see figure 3.

where κ is a coefficient of proportionality. Hence by integrating Eq. (1) and applying Eqs. (3) and (4), this gives an expression for the side-force coefficient:

$$C_{\mathrm{F}_y} = \mathrm{F}_{y,h} \Big/ \left(\frac{1}{2}\rho U_\infty^2 L^2\right) = K \times \frac{\sin(2\psi)}{(2R)^2}, \tag{5}$$

where $R = L/(2r_m)$ is the fineness ratio and $K = \Sigma(\kappa \times z_{c,\mathrm{aft}}/r_m)$ is the moment-of-vorticity coefficient. From Eq. (5), an expression for the yaw-moment coefficient can be defined as follows:

$$C_{\mathrm{M}_z} = K_h \times C_{\mathrm{F}_y} \frac{L_m}{L}, \tag{6}$$

where L_m is the moment arm from the tail plane to a line of action of the force, and K_h is a coefficient of proportionality.

Calibrating the Empirical Model

Figure 2 provides typical examples of measurements of side-force (C_{F_y}) and yaw-moment (C_{M_z}) coefficients for a slender

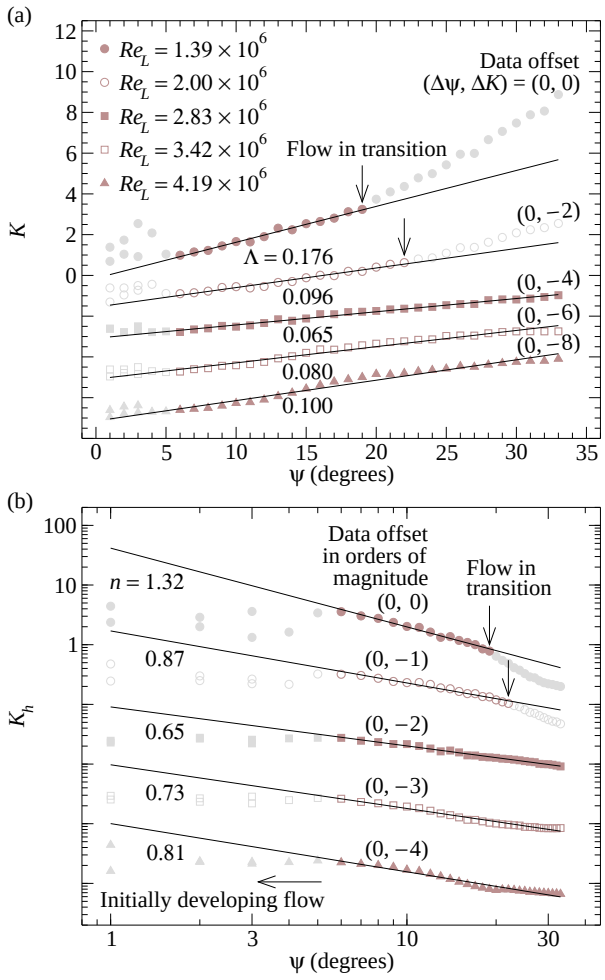

Figure 3. Curve fitting K and K_h of Eq. (7) to Ahn's [2] wind-tunnel data points for a prolate spheroid ($R = 6$ and $L_m = L/2$). The vertical arrows mark a transition in the flow at increasing Reynolds number (Re_L).

hull at incidence up to 33°. By rearranging Eqs. (5) and (6) in terms of K and K_h respectively, and plotting these terms as functions of ψ, the measurements in figure 3 show that, provided the Reynolds number is sufficiently large ($Re_L = LU_\infty/\nu > 2$ million), the coefficient K can be modelled by a straight line and K_h modelled by a power law over a wide range of yaw angles beyond the initially developing flow, viz.

$$K \propto \Lambda\psi \quad \text{and} \quad K_h \propto \psi^{-n}, \tag{7}$$

where $|\psi| > 0$ and the empirical coefficients Λ and n are determined by minimising the root-mean-square (r.m.s.) difference between curve fit and data points. Note that Λ and n are coupled since Eqs. (5) and (6) are coupled.

From Eq. (7), it is possible to use the mean slope Λ (and/or the exponent n) as a measure of moment-of-vorticity growth rate to assess the cross flow around the hull. In the following study, this empirical model is used to interpret the effect of the Reynolds number, fineness ratio, coning motion, experimental hull-support structure (pylon) interference, and deck orientation.

Effect of the Reynolds number

From surface-oil flow visualisation, Ahn [2] identified that transition from laminar to turbulent (cross-flow) separation aft of a 6-to-1 prolate spheroid occurs at a Reynolds number (Re_L) just above 2 million. In figure 3, this flow in transition is accompanied by a widening of the data range which satisfies Eq. (7). A plot of the model coefficients in figure 4 shows that they approach constant values ($\Lambda \simeq 0.085$ and $n \simeq 0.767$) when Re_L is increased from ∼1 million to 4 million.

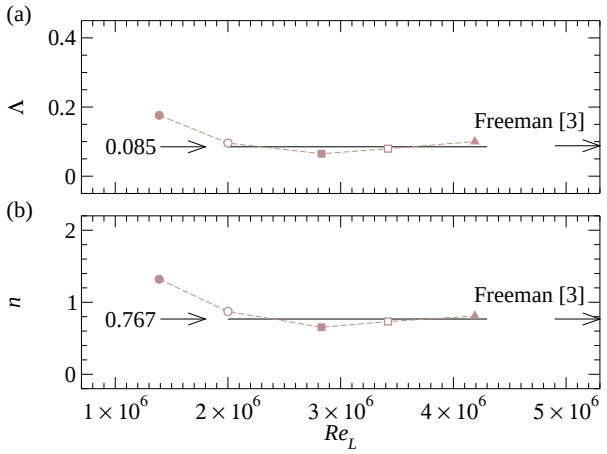

Figure 4. Model coefficients (Λ and n) as functions of Reynolds number (Re_L) for Ahn's [2] wind-tunnel data on a 6-to-1 prolate spheroid (from figure 3).

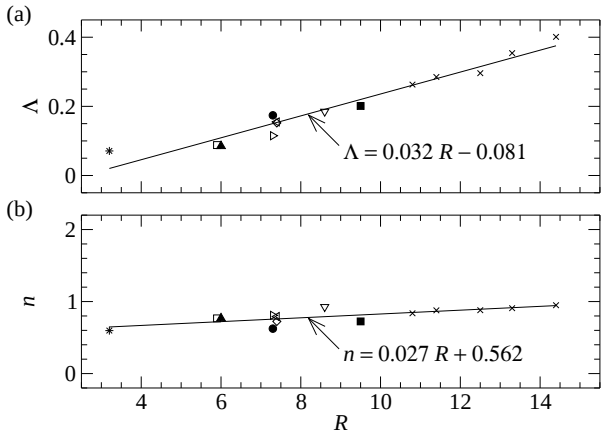

Figure 5. Model coefficients (Λ and n) as functions of fineness ratio (R); see table 1 for description of the symbols.

For larger Reynolds numbers (Re_L ∼12-18 million) tested for a ∼6-to-1 prolate spheroid, inspection of the data of Freeman [3] indicated that $\Lambda(\simeq 0.088)$ and $n(\simeq 0.767)$ are independent of Re_L (also see table 1).

Effect of Fineness Ratio

Table 1 provides a review summary of the moment-of-vorticity growth rate for a collection of axisymmetric bodies [2]-[10] of different fineness ratios (R) operating at Re_L above ∼2 million. The empirical coefficients (Λ and n) are obtained by minimising the r.m.s. difference between curve fit and data points. For yaw magnitudes $|\psi|$ outside the range given in table 1, measurements are either not available or are discarded due to large statistical scatter.

A plot of table 1 in figure 5 shows that Λ and n are increasing functions of R; the data in the range $3 \lesssim R \lesssim 14$ follows a linear trend. Clearly, a more slender hull produces a larger rate-of-change in the coefficients K and K_h.

Effect of Coning Motion

During manoeuvre, an airship or a submersible vehicle may be subject to roll motion in a cross flow — a process described as

Table 1. Cross-flow characteristics of axisymmetric hulls with fineness ratio R operating over a range of incidence angle ψ. No tripping is used to stimulate the nose boundary layer during experiments; $L_m = L/2$. The Reynolds number Re_L is 2 million or more [2]-[10].

Hull geometry / Reference	Test facility / Support structure	R	$\lvert\psi\rvert$	$\sim Re_L$ ($\times 10^6$)	Λ	n	Figure 5 symbol
DRDC aft-body [6]	Wind tunnel / A tail sting	3.2	8°-35°	5	0.071	0.597	$*$
Prolate spheroid - Akron [3]	Wind tunnel / Wires attached to body	5.9	6°-20°	12-18	0.088	0.767	□
Prolate spheroid [2]	Wind tunnel / A tail sting	6.0	6°-33°	2-4	0.085	0.767	▲
DST Group - Joubert [5]	Wind tunnel / A vertical pylon with faring	7.3	5°-30°	5	0.174	0.624	●
NSWCCD - Series 58 [7]	Water basin / Twin struts on body	7.3	5°-18°	5-12	0.115	0.809	▷
Maya/Pirajuba AUV [8]	Towing tank / A mid-body strut with no faring	7.4	3°-25°	2	0.155	0.792	◁
	Towing tank / A mid-body strut with faring	7.4	3°-25°	2	0.152	0.724	◇
DRAPA - SUBOFF [9]	Water basin / Twin struts on body	8.6	3°-18°	14	0.185	0.926	▽
MIT [4]	Water tunnel / A tail sting on a rotating arm	9.5	12°-20°	5	0.201	0.724	■
Underwater vehicle [10]	Towing tank / Twin struts on body	10.8	4°-10°	17	0.263	0.837	×
		11.4	4°-10°	18	0.285	0.878	×
		12.5	4°-10°	20	0.296	0.880	×
		13.3	4°-10°	21	0.354	0.908	×
		14.4	4°-10°	23	0.401	0.949	×

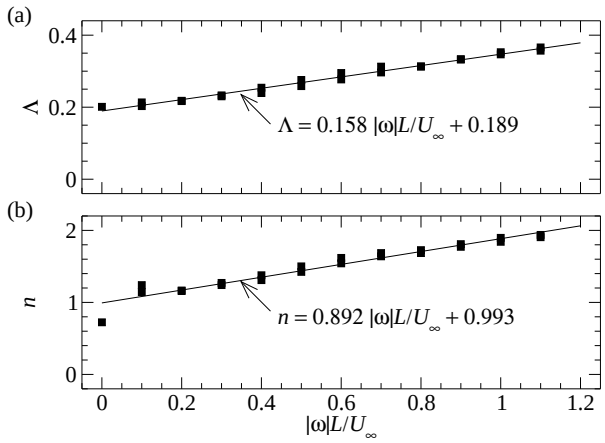

Figure 6. Model coefficients (Λ and n) as functions of roll rate ($|\omega|L/U_\infty$) for Eccles' [4] water-tunnel data (■) on the MIT slender body ($R = 9.5$ and $L_m = L/2$) operating at $Re_L = 5 \times 10^6$.

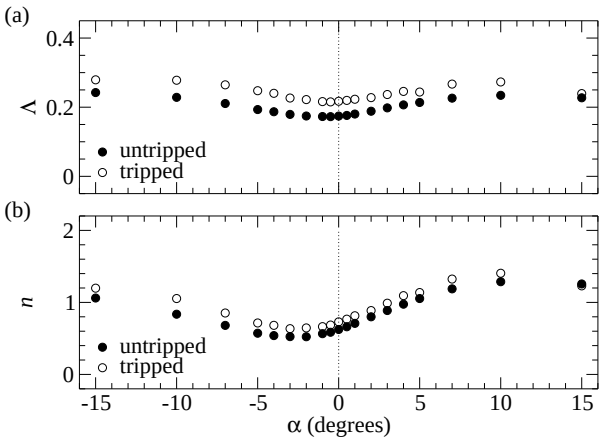

Figure 7. Model coefficients (Λ and n) as functions of pitch angle (α) for Quick's [5] wind-tunnel data on the Joubert hull form ($R = 7.3$ and $L_m = L/2$) operating at $Re_L = 5.2 \times 10^6$ without tripping (●) and with tripping (○) of the nose boundary layer.

coning motion, i.e. the shape of the locus of body-axis rotation about an axis parallel to the free-stream is a cone [4]. For angle of incidence $\psi = 0°$, the motion is pure roll ω (see figure 1).

From flow-field mapping using laser Doppler velocimetry, Eccles [4] showed that the cross-flow vortices are visible for $\psi \gtrsim 10°$ but are highly asymmetric in the presence of roll. In his study, the coning motion is achieved by attaching a slender hull ($R = 9.5$) to a rotating arm via a sting [4]. In figure 6, the empirical coefficients (Λ and n) are obtained by curve-fitting data points in the range $12° \le |\psi| \le 20°$. Inspection shows that Λ and n are linear functions of roll rate ω, where by increasing $|\omega|L/U_\infty$ from 0 up to 1.2 increases Λ and n by a factor of $\sim$2.

Example of Experimental Hull-Support Structure (Pylon) Interference

In laboratory flows, the use of an ancillary support structure requires careful consideration because it can interfere with the cross flow around the hull. For example, on testing with an axisymmetric hull, Quick et al. [5] indicated that their hull-support structure (i.e. a vertical pylon and a pitching arm attached to the lower hull) produced non-negligible asymmetry in the flow. At zero incidence (pitch $\alpha = 0°$ and yaw $\beta = 0°$), the blockage area of the support structure is a factor of 3.2 larger than the frontal area of the hull. This produced a flow offset angle of $\alpha \sim 1.8°$ about the pitch (y') axis and $\beta \sim 0.24°$ about the yaw (z') axis [5]. Clearly, the larger flow offset in pitch (α) is due to the vertical orientation of the pylon support structure.

From their [5] pitch (α, y') and yaw (β, z') components in the body-fixed coordinate system, it is possible to calculate the resultant side-force and yaw-moment coefficients in the cross-flow coordinates (see figure 1) to assess the extent of the bias in the development of the cross flow due to the pylon, viz.

$$C_{F_y} = \sqrt{{C_{F_{y'}}}^2 + {C_{F_{z'}}}^2} = K \times \frac{\sin(2\psi)}{(2R)^2}, \tag{8}$$

$$C_{M_z} = \sqrt{{C_{M_{z'}}}^2 + {C_{M_{y'}}}^2} = K_h \times C_{F_y} \frac{L_m}{L}, \tag{9}$$

where

$$\psi = \sin^{-1}\sqrt{\sin^2(\alpha) + \sin^2(\beta)}. \tag{10}$$

In figure 7, the model coefficients Λ and n of Eq. (7), obtained by curve fitting Eqs. (8) and (9) to the data of [5] in the range $-15° \le \alpha \le 15°$ and $5° \le |\beta| \le 30°$, are plotted as functions of pitch angle α.

The Λ and n distributions in figure 7 show the effect on the moment-of-vorticity growth rate due to the flow offset in pitch (α) produced by the pylon. A slight increase in Λ and n can be observed by stimulating the nose boundary layer with a circumferential ring of transition strip (located at 5% L downstream of the nose of the hull) but this does not change the overall trend for Λ and n (see figure 7).

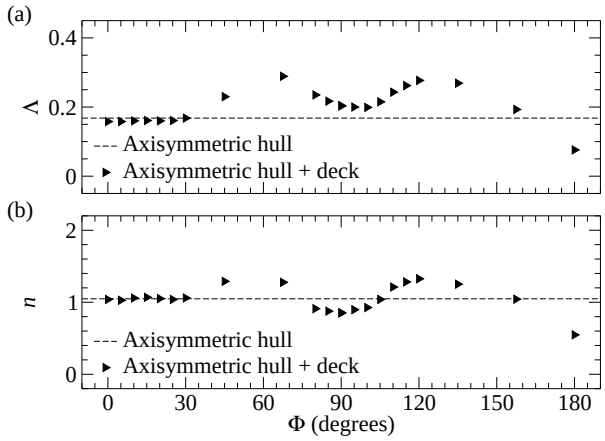

Figure 8. Model coefficients (Λ and n) as functions of deck orientation (Φ) for Marshall's [11] CFD data (---, ▶) on a free-body DRDC-STR hull ($R = 8.75$ and $L_m = L/2$) operating at $Re_L = 23 \times 10^6$.

Effect of adding a Deck to the Hull

In their computational-fluid-dynamics (CFD) study, Marshall et al. [11] demonstrated that the addition of a deck on the hull and the orientation of the deck with respect to the cross flow can affect the surface-flow pattern and wake topology. By changing the orientation angle (Φ), this alters the side force and yaw moment relative to the cross flow, after [11]:

$$C_{\mathrm{F}_y} = C_{\mathrm{F}_{y'}} \sin(\Phi) + C_{\mathrm{F}_{z'}} \cos(\Phi) \quad = K \times \frac{\sin(2\psi)}{(2R)^2}, \qquad (11)$$

$$C_{\mathrm{M}_z} = C_{\mathrm{M}_{y'}} \cos(\Phi) - C_{\mathrm{M}_{z'}} \sin(\Phi) = K_h \times C_{\mathrm{F}_y} \frac{L_m}{L}, \qquad (12)$$

where the subscripts y' and z' denote the pitch and yaw axes in the body-fixed coordinate system, respectively (see figure 1).

In figure 8, the model coefficients Λ and n of Eq. (7), obtained by curve fitting Eqs. (11) and (12) to the data of [11] in the range $10^\circ \leq \psi \leq 30^\circ$, are plotted as functions of the deck-orientation angle. For $\Phi = 0^\circ$, the cross flow approaches the deck head on (refer to figure 1). Inspection of figure 8 shows that, for $0^\circ \leq \Phi \lesssim 30^\circ$, the trends are nearly the same with and without the deck. However, the trends indicate clear departure when Φ is increased from 30° to 180°, with local maxima observed at $\Phi \simeq 60^\circ$ and 120°; the minimum is observed at $\Phi = 180^\circ$, where the deck is directly opposite to the incidence flow and acts as an aft-body [11].

Conclusions

An analytical-empirical model has been developed and is used to study the characteristics of side force on slender hulls in a cross flow. The key findings obtained from this study are summarised as follows.

- For Reynolds number $Re_L \gtrsim 2$ million, the moment-of-vorticity growth rate (Λ or n defined by Eq. (7)) for a 6-to-1 prolate spheroid is independent of Re_L. For axisymmetric bodies operating at $Re_L \gtrsim 2$ million, the growth rate (Λ or n) increases linearly with the fineness ratio (R) of the hull.
- The cross-flow vortices are generally visible for incidence angle $|\psi| \gtrsim 10^\circ$ but are highly asymmetric in the presence of roll. In coning motion, Λ or n increases linearly with the roll rate. For a slender hull of $R = 9.5$, increasing the roll rate $|\omega| L/U_\infty$ from 0 to 1.2 increases Λ or n by a factor of $\sim$2.
- The cross flow is sensitive to ancillary components of the hull. For example, an experimental pylon support structure can bias the moment-of-vorticity growth rate (Λ or n) depending on the location of the pylon. A deck, depending on its azimuthal orientation Φ, can produce local maxima (and minimum) in the moment-of-vorticity growth rate.

Acknowledgement

The author offers his sincere thanks to Howard Quick, Gregory Seil and Matteo Giacobello for useful discussions.

References

[1] Jeans, T. L. *An estimation method for the normal force distribution on slender axisymmetric bodies with tapered tails*. Ph.D. Thesis, Department of Mechanical Engineering. University of New Brunswick, Canada, 2007.

[2] Ahn, S. *An experimental study of flow over a 6 to 1 prolate spheroid at incidence*. Ph.D. Thesis, Aerospace Engineering Department, Virginia Polytechnic Institute and State University, Blacksburg, VA, 1992.

[3] Freeman, H. B. Force measurements on a 1/40-scale model of the US airship Akron. TR432, NACA, 1932.

[4] Eccles, T. J. *Measurement of hydrodynamic forces and moments and flow field mapping of a model in coning motion*. M.S. Thesis, MIT, 1990.

[5] Quick, H., Widjaja, R., Anderson, B., Woodyatt, B., Snowden, A. D. & Lam, S. Phase I experimental testing of a generic submarine model in the DSTO low speed wind tunnel. TN1101, DSTO, 2012.

[6] Mackay, M. Wind tunnel experiments with a submarine afterbody model. DRDC-Atlantic TM2002-194, 2003.

[7] Van Randwijck, E. F. & Feldman, J. P. Results of experiments with a segmented model to investigate the distribution of the hydrodynamics forces and moments on a streamlined body of revolution at an angle of attack or with a pitching angular velocity. NSWCCD-50-TR-2000/008, Naval Surface Warfare Center Carderock Division, 2000.

[8] Dantas J. L. D., de Barros, E. A., Boas, F. V., Mutscheler F. A. & Umeda C. H. Experimental research on AUV manoeuvrability. *21st International Congress of Mechanical Engineering*, Natal, RN, Brazil, 2011.

[9] Roddy, R. F. Investigation of the stability and control characteristics of several configurations of the DRAPA SUBOFF model (DTRC model 5470) from captive-model experiments. DTRC/SHD-1298-08, 1990.

[10] Praveen, P. C. & Krishnankutty, P. Study on the effect of body length on the hydrodynamic performance of an axi-symmetric underwater vehicle. *Indian Journal of Geo-Marine Sciences*, 2013, 42(8):1013–1022.

[11] Marshall, C. R., Jeans, T. L., Holloway, G. L. & Watt, G. D. Hydrodynamic forces and moments on slender axisymmetric bodies with decks in translation. *52nd Aerospace Sciences Meeting*, 2014, AIAA SciTech 2014-1270.